

Numerical simulation of one-dimensional perovskite solar cell model

Saidatul Nur Aisyah Tun Sakinah¹, Rahifa Ranom¹, Siti Hajar Basmin², Lee Jin Yao¹

¹Solar PV System and Smart Grid Research Laboratory, Department of Electrical Engineering, Faculty of Electrical Technology and Engineering (FTKE), Universiti Teknikal Malaysia Melaka (UTeM), Melaka, Malaysia

²OSI Optoelectronics Sdn. Bhd, Johor, Malaysia

Article Info

Article history:

Received Apr 12, 2023

Revised Oct 19, 2023

Accepted Feb 12, 2024

Keywords:

Drift-diffusion

Mathematical modeling

One-dimensional

Perovskite

Solar cell

ABSTRACT

Perovskite solar cell (PSC) is one of the advanced third-generation solar cells that have rapid efficiencies but instability issues in terms of air, moisture, and UV light sensitivity becomes a barrier to commercialization. The instability issue is due to the charge accumulation at the interface of the PSC reducing its efficiency. This research focuses on the operation of PSCs through a one-dimensional (1D) drift-diffusion model for planar heterojunction PSCs. The model also accounts for the electric potential by Poisson's equation, the ion generation, and the recombination rate. The method of lines technique is applied to solve the model for the perovskite layer numerically using the finite difference method which is then solved forward in time using the 'ode15s' solver in MATLAB. It is highlighted that the comparison with the experimental data from the reference shows good agreement. The effect of parameter thickness variation of the perovskite layer upon the efficiency of PSCs is analyzed. The result shows that the best efficiency obtained is 19.77% obtained at thickness 0.25 μm . The results may prove useful for a guideline of the cell thickness that predicts the perovskites cell performance.

This is an open access article under the [CC BY-SA](#) license.



Corresponding Author:

Saidatul Nur Aisyah Tun Sakinah

Solar PV System and Smart Grid Research Laboratory, Department of Electrical Engineering

Faculty of Electrical Technology and Engineering (FTKE), Universiti Teknikal Malaysia Melaka (UTeM)

Melaka, Malaysia

Email: m012020012@student.utem.edu.my

1. INTRODUCTION

The solar cell is a device that converts light energy into photovoltaic energy. The usage of solar cells that are pollution-free, low-cost, and renewable energies are the main advantages that contribute to a positive effect on living and economics [1], [2]. Perovskite solar cell (PSC) is one of the advanced technologies developed from the dye-sensitized solar cell (DSSC) that is categorized as a third-generation solar cell [3], [4]. Since 2009, the perovskites solar cell has been remarkable due to cost-effectiveness, high-power conversion efficiency, strong optical absorption, and ease of fabrication [5].

However, the stability issue in terms of moisture, light, toxicity level, and thermal lead to current-voltage hysteresis, reducing the efficiency of the PSC [6]–[8]. The instability issue is related to the mechanisms of charge transport via diffusion (charge density gradient) and advection (by an electric field) and charge release at the interface between layers during ion migration which dominates the global electrical field [8]–[10]. The movement of the charge transport is related to the dynamic physics of the PSC which requires a proper mathematical model that describes charge transport layers [11].

Various works perform the modeling of the charge accumulation at the interface of the PSC. Based on the finding from Neukom *et al.* [12] considering the ion and charge traps that are capable of relating the hysteresis behavior in PSCs using experimental and numerical simulation Fluxim but the mobility of ion migration is assumed to be constant and the concentration of upper limit boundaries does not being imposed. The impedance spectroscopy technique is applied by Khan *et al.* [13] to probe the interfacial surface of the perovskite layer to study the interface charge accumulation, recombination losses, and charge transport mechanism but the technique is highly sensitive. The finding shows that the organohalide type MAPBI₃ contributes to low interfacial recombination compared to organohalide ((FAPbI₃)_{0.85} (MAPbBr₃)_{0.15}) [13]. The equivalent electrical circuit for modeling the PSC involves the series of two diodes that represent the active junction at the holes transport layer and electrons transport layer as the perovskite layer absorbs the sunlight energy [14], [15]. Using equivalent circuit modeling to study the physics of PSC is too straightforward and lacks the electrochemical behavior of PSC while the atomistic density functional theorem (DFT) requires high computational cost and applies to a limited number of atoms [16]. The work from Courtier *et al.* [16] shows that the transport layer properties affect the performance of the PSC depending on the degree of the hysteresis using the extension of the numerical scheme from. To fill in the gap, the drift-diffusion model is found to be the best model for modeling the PSC due to the ability to account for the dynamic physics of the charge transport model involving the drift and diffusion mechanisms and potential difference with extremely small Debye layer [16], [17].

The solution to the drift-diffusion equation may vary such as using a solar cell simulator (SCAPS-1D [18], [19], wxAMPS [20], IonMonger [21]) directly or using the numerical method and asymptotic analysis [22], [23]. The challenge that arises when using simulators is the generation profile needed using the transfer matrix method [19]. The drift-diffusion equations consisted of the coupled ordinary differential equations (ODE) and partial differential equation (PDE) [22], [24]. Instead of using the complex asymptotic analysis [16], [17], the method of line (MOL) technique is proposed to solve the drift-diffusion equations which is also the main contribution in this research. The method of the line has advantages in decoupling the spatial and temporal discretization processes [25]. The result is compared with the reference [24] for validation purposes. Next, the thickness of the perovskite layer (absorber) is varied to analyze the effect on the efficiency of the PSC. The main contribution to the research is the MOL technique to solve the perovskites solar cells model.

2. MATHEMATICAL MODEL AND NUMERICAL PROCEDURE

This section discusses the mathematical model of the PSC and the numerical procedure to solve the model.

2.1. Modeling of the perovskite solar cell

Figure 1 shows the schematic diagram of solar cells in which the perovskite is sandwiched between the holes transport layer (HTL) and electrons transport layer (ETL). The holes transport layer (HTL) is made up of spiro-OMETAD and the ETL is made up of titanium oxide [24]. The p and n represent holes and electrons, respectively, where L represents the perovskite thickness.

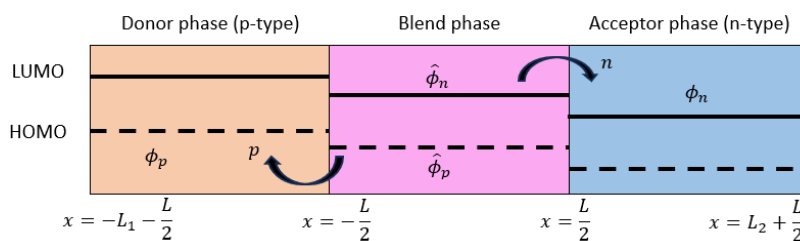


Figure 1. The schematic diagram of the PSC. The solid line represents the highest occupied molecular orbital (HOMO) while the least unoccupied molecular orbital (LUMO) (dashed line). The p -type donor layer $(-L_1 - \frac{L}{2} < x < -\frac{L}{2})$, the perovskite $(-\frac{L}{2} < x < \frac{L}{2})$ and the n -type acceptor layer $(\frac{L}{2} < x < L_2 + \frac{L}{2})$

The sunlight is absorbed in the perovskites layer which has a highly ordered crystalline structure comprised of distinct conduction band edges, $\hat{\phi}_n$, and valence band edges, $\hat{\phi}_p$ that are divided by a band gap [24]. The organics materials of the donor phase (p -type) and acceptor phase (n -type) have no distinct band structure and are amorphous [24]. LUMO portrays the conduction band, and the energy of the acceptor is

denoted as ϕ_n while HOMO portrays the valence band, and the energy of the donor is denoted as ϕ_p . The electrons are excited into the LUMO, leaving a hole in the HOMO, resulting in the conduction process due to the excited electrons and hole movement between the HOMO and LUMO respectively on the adjacent molecules. The dynamic modeling for PSCs in this research describes the electric potential by the poisson equation, the charge densities and current densities for holes and electrons by drift-diffusion equations, continuity equations of ions, and the electron-hole pair recombination and generations are also accounted [17]. Therefore, the mathematical model of charged ion species (p and n) which diffuse by the ionic concentration gradient and advect by an electric field in the perovskite layer $\left(-\frac{L}{2} < x < \frac{L}{2}\right)$ in (1)–(3) [24].

Poisson's equation:

$$\frac{\partial^2 \phi}{\partial x^2} = \frac{q}{\epsilon} (n - p) \quad (1)$$

Drift-diffusion equations:

$$\frac{\partial p}{\partial t} + \frac{1}{q} \frac{\partial J^p}{\partial x} = \alpha (np - n_i^2); \quad J^p = -qD_p \left(\frac{\partial p}{\partial x} + \frac{qp}{kT} \frac{\partial \phi}{\partial x} \right) \quad (2)$$

$$\frac{\partial n}{\partial t} - \frac{1}{q} \frac{\partial J^n}{\partial x} = \alpha (np - n_i^2); \quad J^n = qD_n \left(\frac{\partial n}{\partial x} - \frac{qn}{kT} \frac{\partial \phi}{\partial x} \right) \quad (3)$$

The p, n are the density of holes and electrons, respectively, J^n and J^p are the current density of electrons and holes, ϕ is the electric potential, $\alpha(np - n_i^2)$ is the recombination rate. The recombination rate consists of α , the radiative recombination coefficient, and, n_i the doping density. The type of recombination considered in this work is band-to-band radiative recombination which is the recombination that naturally occurs in PSCs [21]. The recombination occurs when the electrons in the conduction band recombine with holes in the valence band resulting in the emission of a photon in between the band gap [22]. Meanwhile, q is the elementary charge, ϵ is the permittivity, D_n and D_p are the diffusivity of electrons and holes, k is the Boltzmann constant and T is the temperature, respectively. The total current throughout the device is $J = J^n + J^p$.

The boundary conditions at the interface of the perovskite layer to the acceptor phase, $x = -\frac{L}{2}$ and at the interface of the perovskite layer to the donor phase, $x = \frac{L}{2}$ in (4) and (5), respectively:

$$\hat{\phi}|_{x=-\frac{L}{2}} = \phi_l, \quad p|_{x=-\frac{L}{2}} = \epsilon_p \pi_0, \quad n_x|_{x=-\frac{L}{2}} = -\frac{\pi_0}{L} \quad (4)$$

$$\hat{\phi}|_{x=\frac{L}{2}} = \phi_r, \quad n|_{x=\frac{L}{2}} = \epsilon_n \pi_0, \quad p_x|_{x=\frac{L}{2}} = \frac{\pi_0}{L} \quad (5)$$

where ϵ_p, ϵ_n are the valence band density between the donor and perovskite layer and the conduction band density between the acceptor and perovskite layer, respectively. Here, π_0 is an assumption of the typical charge density that carries a current, ϕ_l and ϕ_r are the potential differences at $x = -\frac{L}{2}$ and at $x = \frac{L}{2}$ of the device, respectively. Here, it is assumed that the total voltage flow at the interface of perovskites at both phases (acceptor and donor) is the same. The potential at $x = 0$ is set to $\hat{\phi}|_{x=0} = 0$, which complies the Kirchhoff's Voltage Law [24]. The initial condition (at $t = 0$) for the potential is fitted to the experimental data from [21].

$$\hat{\phi}(x, 0) = V_0(661.3x^7 - 115.1x^6 + 194.2x^5 + 33.3x^4 - 17.13x^3 - 2.293x^2 + 0.3135x + 0.026) \quad (6)$$

The potential V_0 is set equal to the thermal voltage $V_0 = \frac{q}{kT}$ which is equivalent to 20V. At $x = -\frac{L}{2}$, only the holes, p are allowed into the donor phase, which is assumed to equal to $\epsilon_p \pi_0$ while at $x = \frac{L}{2}$, only the electrons, n exited to enter the acceptor phase and are set to $\epsilon_n \pi_0$.

2.2. Nondimensionalisation

In (1) to (5) were converted into the dimensionless model and the numerical simulation was solved in dimensionless. The charge density, the cell thickness, and the potential are scaled to the typical charge carrier density, $\pi_0 = 7.9 \times 10^{23} m^{-3}$, the width of perovskites solar cell (L), and the thermal voltage $\frac{kT}{q}$, respectively [21]. In this work, the hole and electron density are assumed to be the same as carrier density, π_0 .

The superscript tilde denotes the parameter is dimensionless. The scaling form (1) to (5) is as follows (note that the tilde denotes the dimensionless variables):

$$\tilde{n} = \pi_0 n, \tilde{p} = \pi_0 p, \tilde{t} = \tau t, \tilde{\phi} = \frac{kT}{q} \hat{\phi}, \tilde{x} = Lx, n_i^2 = \pi_0^2 \quad (7)$$

Here we assume that both holes and electrons diffuse at the same diffusion rate $D_p = D_n = D_0$, where D_0 is the typical diffusivity of the charges in which the time scaling of the cell operation is:

$$\tau = \frac{L^2}{D_0^2} \quad (8)$$

which leads to the following dimensionless equations:

$$\frac{\partial^2 \tilde{\phi}}{\partial \tilde{x}^2} = \frac{1}{\lambda^2} (\tilde{n} - \tilde{p}) \quad (9)$$

$$\frac{\partial \tilde{n}}{\partial \tilde{t}} = \frac{\partial}{\partial \tilde{x}} \left(\frac{\partial \tilde{n}}{\partial \tilde{t}} - \tilde{n} \frac{\partial \tilde{\phi}}{\partial \tilde{x}} \right) + \gamma (\tilde{n} \tilde{p} - 1) \quad (10)$$

$$\frac{\partial \tilde{p}}{\partial \tilde{t}} = \frac{\partial}{\partial \tilde{x}} \left(\frac{\partial \tilde{p}}{\partial \tilde{t}} + \tilde{p} \frac{\partial \tilde{\phi}}{\partial \tilde{x}} \right) + \gamma (\tilde{n} \tilde{p} - 1) \quad (11)$$

with boundary conditions:

$$\tilde{\phi}|_{\tilde{x}=-\frac{1}{2}} = \frac{\phi_l}{V_0}, \tilde{p}|_{\tilde{x}=-\frac{1}{2}} = \varepsilon_p, \tilde{n}|_{\tilde{x}=-\frac{1}{2}} = -1 \quad (12)$$

$$\tilde{\phi}|_{\tilde{x}=\frac{1}{2}} = \frac{\phi_r}{V_0}, \tilde{n}|_{\tilde{x}=\frac{1}{2}} = \varepsilon_n, \tilde{p}|_{\tilde{x}=\frac{1}{2}} = 1 \quad (13)$$

The dimensionless parameters in (9) to (11) are defined by:

$$\lambda = \sqrt{\frac{\varepsilon kT}{\pi_0 q^2 L^2}}, \gamma = \frac{\alpha L^2 \pi_0}{D_0} \quad (14)$$

where λ and γ are the ratio of the Debye length to the width of the perovskite layer and the ratio of the typical charge diffusivity in bulk density to the typical diffusivity of the charges in the perovskite, respectively. The J-V curve is an important tool to determine the efficiency of the perovskites solar cell. The J-V curve function shown in (15) is used referred from reference [24], with the assumption that only the perovskite layer is considered. The relationship between the current density, J , and voltage, V has been derived by Soedergren *et al.* [26] based on electron diffusion and is given by:

$$J = J_{sc} - \frac{q D_0 \pi_0}{L_D} \tanh\left(\frac{L}{L_D}\right) \left(\exp\left(\frac{qV}{kTm}\right) - 1 \right) \quad (15)$$

where the short-circuit current density, J_{sc} is:

$$J_{sc} = \frac{q \Phi L_D \epsilon}{1 - L^2 \epsilon^2} \left(-L_D \epsilon + \tanh\left(\frac{L}{L_D}\right) + \frac{L_D \epsilon \exp(-\epsilon L)}{\cosh\left(\frac{L}{L_D}\right)} \right) \quad (16)$$

Here, Φ is the light intensity; L_D is the diffusion length of the electrons; ϵ the light absorption coefficient, and m is the ideality factor. The maximum voltage, V_m and current density, J_m , short circuit current density, J_{sc} , and open circuit voltage, V_{oc} are extracted from the J-V curve and used to calculate the fill factor, FF , and the efficiency, η of the PSC by (17) and (18):

$$FF = \frac{V_m J_m}{J_{sc} V_{oc}} \quad (17)$$

$$\eta(\%) = \frac{V_{oc} J_{sc} FF}{P_{in}} \times 100 \quad (18)$$

2.3. Numerical simulation: method of line technique

The MOL technique converts partial differential equations (PDEs) into a set of ordinary differential equations (ODEs) [16], [27]. The ODEs are obtained by discretizing the derivatives of spatial variables in (11) to (16) using finite difference approximation with applied boundary conditions. The parameters of the perovskites solar cell are listed in Table 1 [24], [26], [28]. The spatial variables in (9) to (14) are discretized using the centered difference approximation in (19) to (21) which offers a small tolerance for error and high accuracy.

$$\frac{\partial p_i}{\partial t} = \frac{1}{h^2} \left[p_{i+1} - 2p_i + p_{i-1} + \frac{(p_i + p_{i+1})(\phi_{i+1} - \phi_i) - (p_i + p_{i-1})(\phi_i - \phi_{i-1})}{2} \right] + \gamma(n_i p_i - 1) \quad (19)$$

$$\frac{\partial n_i}{\partial t} = \frac{1}{h^2} \left[n_{i+1} - 2n_i + n_{i-1} - \frac{(n_i + n_{i+1})(\phi_{i+1} - \phi_i) - (n_i + n_{i-1})(\phi_i - \phi_{i-1})}{2} \right] + \gamma(n_i p_i - 1) \quad (20)$$

$$\frac{\partial \phi_i}{\partial x} = \frac{1}{h^2} [\phi_{i+1} - 2\phi_i + \phi_{i-1}] - \frac{1}{\lambda^2} (n_i - p_i) \quad (21)$$

These equations can be expressed in general matrix form:

$$M \frac{\partial u}{\partial t} = Au + f(x, t) \quad (22)$$

In (19) and (21) is transformed into matrix form shown in (22) for $i = 1, 2, 3 \dots m$. The solution vector denotes as u , the time-dependent mass matrix, M , (where 1 denotes the time derivative and 0 denotes no time derivative), A is the discretization of the differentiation matrix in (9) to (11) with the boundary equations from (12) and (13), while f represents the generation and recombination of the charge density of holes and electrons in (10) and (11) and the net of charge densities in (9). The ODEs (19) to (21) in the matrix form (22) is then solved by using the implicit ODE solver 'ode15s' in time forward via MATLAB with the resolution of the system, $m = 101$. Table 1 shows the PSC parameters for the simulation.

Table 1. The parameters of the PSC [24], [27], [28]

Parameter	Symbol	Value	Unit
Permittivity	ε	$1000\varepsilon_0$	$A^2 s^4 kg^{-1} m^{-3}$
Diffusivity of holes	D_p	2.5×10^{-9}	$m^2 s^{-1}$
Diffusivity of electrons	D_n	2.5×10^{-9}	$m^2 s^{-1}$
Boltzmann constant	k	1.38×10^{-23}	$m^2 kg s^{-2} K^{-1}$
Elementary charge	q	1.603×10^{-19}	C
Thickness	L	0.5×10^{-6}	m
Radiative recombination coefficient	α	1.1×10^{-16}	$m^{-3} s^{-1}$
Light intensity	Φ	1.5×10^{21}	$m^{-2} s^{-1}$
Diffusion length	L_D	1.4×10^{-3}	m
Light absorption coefficient	ϵ	1.2×10^7	m^{-1}
Ideality factor	m	1.3	

The dimensionless initial conditions are fitted from [24] resulting in (23) for holes and (24) for electrons:

$$\tilde{p}(\tilde{x}, 0) = 315.9x^7 + 142.2x^6 - 71.48x^5 - 35.19x^4 + 6.079x^3 + 2.251x^2 - 0.06481x + 1.05 \quad (23)$$

$$\tilde{n}(\tilde{x}, 0) = 175x^8 - 62.77x^7 - 70.01x^6 + 3.829x^5 + 7.253x^4 - 1.403x^3 - 0.2368x^2 - 0.006944x + 1.064 \quad (24)$$

3. RESULTS AND DISCUSSION

The result and discussion for the charge densities against thickness and the effect of the thickness variation on the efficiency of the PSC are discussed in this section. Figure 2 discovers the comparison of the simulation results (solid lines) and experimental data (circles) [24] for dimensionless electrons (blue color) and holes (red color) densities for $L = 0.5 \mu m$.

Figure 2 shows the comparison of holes (p) and electrons (n) densities between the experimental data [24] and simulation results obtained for $0.5 \mu m$ cell thickness in dimensionless form. The simulation compares reasonably well to the experimental data. At $\tilde{x} = -0.5$ (the interface boundary between the hole transport layer (HTL) and perovskite layer), the electron density is increased, and the hole's density is decreased. At the interface of perovskite and HTL $\tilde{x} = -0.5$, the charge separation occurs which allows only holes to get into the HTL layer while the electron remains in the perovskite layer. Meanwhile, it is vice versa for the density profiles $\tilde{x} = 0.5$ (the interface boundary between the electrons transport layer (ETL) and

perovskite layer). The charge accumulation model can be shown at the interface of the perovskite layer with the electrons transport layer (ETL) at $\tilde{x} = 0.5$ and the holes transport layer (HTL) at $\tilde{x} = -0.5$.

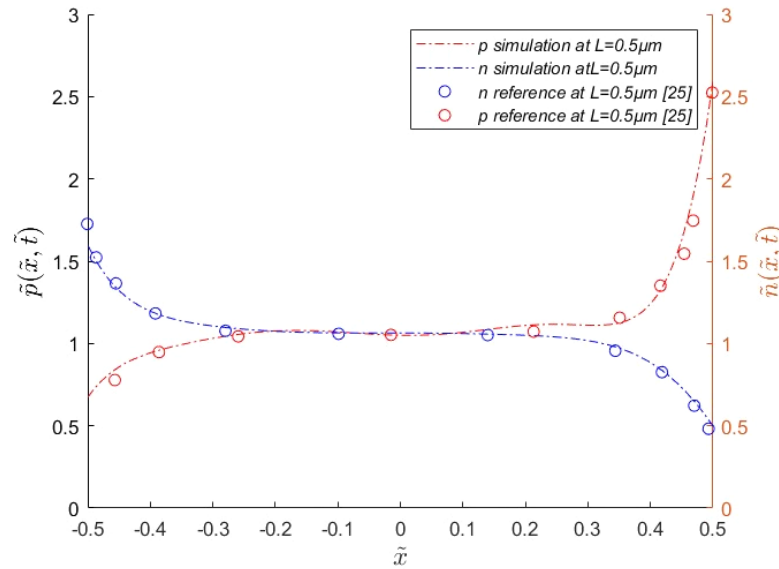


Figure 2. The comparison of the simulation results (solid lines) and experimental data (circles) [24] for dimensionless electrons (blue color) and holes (red color) densities for $L = 0.5 \mu\text{m}$

3.1. The effect of thickness variation of perovskite layer upon cell performance

The perovskite layer thickness is varied from $0.15 \mu\text{m}$ to $0.45 \mu\text{m}$ as referred to [29]. The value of the dimensionless parameters based on thickness is listed in Table 2.

Table 2. The dimensionless parameters of the PSC

Thickness, $L (\mu\text{m})$	γ	λ
0.15	1.1×10^{-3}	1.004×10^{-1}
0.25	3.0×10^{-3}	3.62×10^{-2}
0.35	5.8×10^{-3}	1.84×10^{-2}
0.45	9.6×10^{-3}	1.12×10^{-2}
0.5	1.18×10^{-2}	9×10^{-3}

where λ and γ are the ratios of the Debye length to the width of the perovskite layer and the ratio of the typical charge diffusivity in bulk density to the typical diffusivity of the charges in the perovskite. Based on Table 2, the thickness of $0.15 \mu\text{m}$ has the lowest value of γ , that is 1.1×10^{-3} and increases to 9.6×10^{-3} as the thickness increases to $0.45 \mu\text{m}$. It shows that the recombination factor across the diffusion length slightly increases as the thickness increases in (10) and (11). At $0.15 \mu\text{m}$, the value of λ is 1.0004×10^{-1} and reduces to 1.12×10^{-2} when thickness increases to $0.45 \mu\text{m}$ demonstrates that the ratio of Debye length (charge separation length) to the diffusion length decreases as thickness increases in (9). It allows more charges to diffuse toward the interface boundary (HTL/perovskite and perovskite/ETL).

Figure 3 shows the variation of thicknesses are $0.25 \mu\text{m}$, $0.35 \mu\text{m}$, $0.45 \mu\text{m}$ and $0.5 \mu\text{m}$ which were scaled to dimensionless thickness, $\tilde{x} = -0.5$ to $\tilde{x} = 0.5$ by the scaling of (7). The results indicate that the higher the thickness, the electron and hole densities are slightly lower. For instance, a cell thickness of $0.15 \mu\text{m}$ has the highest electron and hole density value compared to a cell thickness of $0.45 \mu\text{m}$ which has the lowest electron and hole density value because of the increasing recombination process that can be related to γ in scaling from (14). A higher thickness of perovskites affects the ratio of recombination rates, thus reducing the charge densities of PSCs [30]. The reduction of the charge densities occurs when the perovskite's thickness is higher (the relation can be seen in (2) and (3)) and produces lower current density.

Figure 4 discovers the effect of varied thickness on the concentration of the charge densities as time increases. The charge densities of the holes and electrons are more concentrated at $L = 0.25 \mu\text{m}$ refer Figure 4(a) compared to the charge densities at $L = 0.5 \mu\text{m}$ as shown in Figure 4(d). At the interface of the perovskite and

holes transport layer, the density of the holes becomes steeper as the thickness from $L = 0.25 \mu\text{m}$ increases to $L = 0.5 \mu\text{m}$ (refer Figure 4(a)–(d)) due to the effect of the Debye layer [30]. The situation at the interface of the perovskites and electrons transport layer also can be seen that the electrons densities become steeper from thicknesses $L = 0.25 \mu\text{m}$ to $L = 0.5 \mu\text{m}$ due to decreasing ratio of Debye layer. The permittivity gives an effect to the potential difference, ϕ in (2) and (3) for holes and electrons and results in a different level of current density.

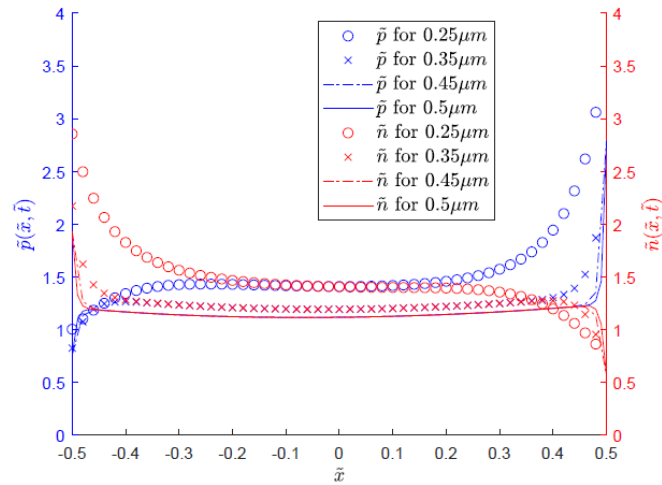


Figure 3. The dimensionless electron and hole densities for various thicknesses ($0.15 \mu\text{m}$, $0.25 \mu\text{m}$, $0.35 \mu\text{m}$, and $0.45 \mu\text{m}$) at time $t = 5 \times 10^{-6}\text{s}$

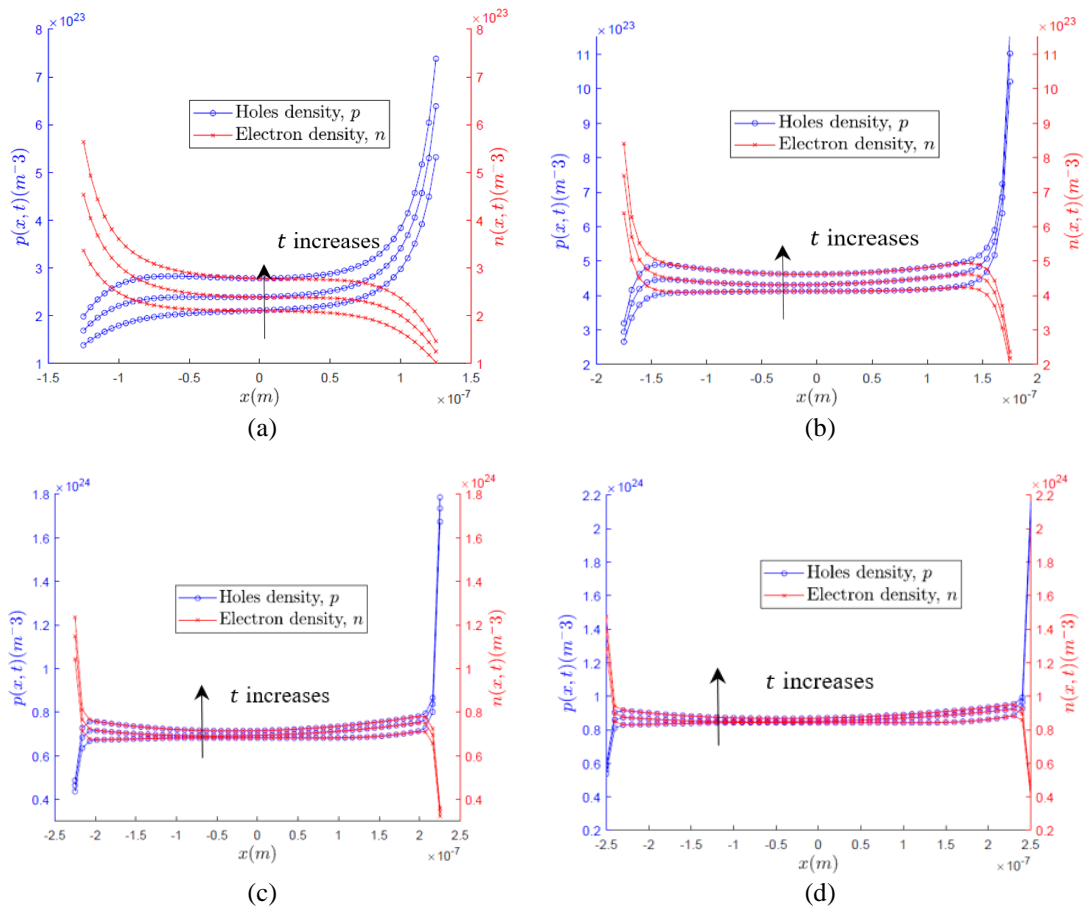


Figure 4. The dimensional holes and electron densities for: (a) $L = 0.25 \mu\text{m}$, (b) $L = 0.35 \mu\text{m}$, (c) $L = 0.45 \mu\text{m}$, and (d) $L = 0.5 \mu\text{m}$

Figure 5 illustrates the current density, J , and voltage, V curve for $0.15\ \mu\text{m}$, $0.25\ \mu\text{m}$, $0.35\ \mu\text{m}$, $0.45\ \mu\text{m}$ and $0.5\ \mu\text{m}$. The maximum voltage, V_m and current density, J_m , short circuit current density, J_{sc} and open circuit voltage, V_{oc} are extracted and tabulated in Table 3 which demonstrates the efficiency of different thicknesses. The value of the efficiency of the PSC is the lowest at thickness $0.15\ \mu\text{m}$, which is 19.19% because the electron and holes move toward respective layers with too short distances with high charge densities. The efficiency started to increase from 19.19% to 19.77% as the perovskite thickness increased from $0.15\ \mu\text{m}$ to $0.25\ \mu\text{m}$, due to high charge densities of holes and electrons and reduced the recombination and increasing ratio of Debye layer. However, the efficiency of the perovskites started to reduce from 19.33% to 19.08% at a thickness of $0.35\ \mu\text{m}$ to $0.5\ \mu\text{m}$, because the holes and electrons started to recombine while traveling toward selective layers respectively and reducing the ratio of Debye layer. As a result, the charge densities of holes and electrons started to decrease shown in Figure 4. Based on the efficiency result on different thicknesses in Table 3, showing that the efficient thickness of perovskite ranges from $0.25\ \mu\text{m}$. Hence, thickness plays an important role in affecting the performance of the solar cell.

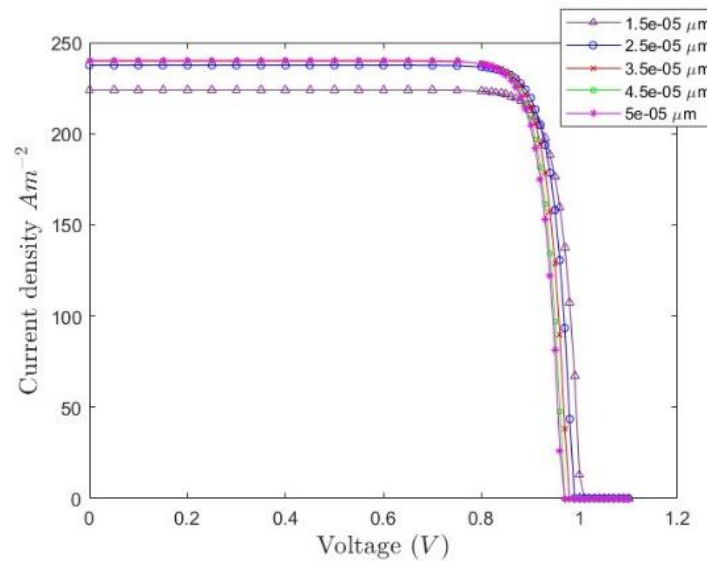


Figure 5. The J-V Characteristic curve for different thicknesses

Table 3. The calculation of efficiency of the perovskites solar cell based on different thicknesses

Thickness, L (μm)	J_{sc} (A m^{-2})	V_{oc} (V)	J_m (A m^{-2})	V_m (V)	FF	η (%)
0.15	223.92	1.01	213.175	0.9	0.8483	19.19
0.25	237.59	0.99	219.663	0.9	0.8405	19.77
0.35	239.87	0.98	214.772	0.9	0.8223	19.33
0.45	240.251	0.97	238.607	0.8	0.8191	19.09
0.50	240.296	0.97	238.469	0.8	0.8185	19.08

4. CONCLUSION

A drift-diffusion model of a one-dimensional solar cell in the perovskite layer is presented and is solved numerically. The charge densities of holes and electrons' behavior across the thickness are shown. The smaller the thickness of the cell the lower the cell efficiency. The best efficiency obtained from the result is 19.77% at a thickness of $0.25\ \mu\text{m}$ which is proven that the optimum thickness to achieve maximum efficiency, but the thickness of perovskite is still acceptable until $0.5\ \mu\text{m}$. The model would be useful as a guideline for the thickness of cells that predicts the perovskite cell performance. However, the simulation can be improved by investigating the behavior of charge density across the three layers of the solar cells. Therefore, the folding technique is suggested to improve the numerical scheme of holes and electrons for all phases for future work.

ACKNOWLEDGEMENTS

The authors thank the Ministry of Higher Education Malaysia and Universiti Teknikal Malaysia Melaka for research and financial support under the grant FRGS/1/2020/STG06/UTEM/02/2/F00414.

REFERENCES




- [1] M. H. Ahmadi *et al.*, "Solar power technology for electricity generation: A critical review," *Energy Science & Engineering*, vol. 6, no. 5, pp. 340–361, Sep. 2018, doi: 10.1002/ese3.239.
- [2] J. Ajayan, D. Nirmal, P. Mohankumar, M. Saravanan, M. Jagadesh, and L. Arivazhagan, "A review of photovoltaic performance of organic/inorganic solar cells for future renewable and sustainable energy technologies," *Superlattices and Microstructures*, vol. 143, p. 106549, Jul. 2020, doi: 10.1016/j.spmi.2020.106549.
- [3] I. van Beuzekom, B.-M. Hodge, and H. Slootweg, "Projecting solar photovoltaic efficiencies from lab to market," in *2018 IEEE International Energy Conference (ENERGYCON)*, Jun. 2018, doi: 10.1109/energycon.2018.8398813.
- [4] J. Luceño-Sánchez, A. Díez-Pascual, and R. P. Capilla, "Materials for Photovoltaics: State of Art and Recent Developments," *International Journal of Molecular Sciences*, vol. 20, no. 4, p. 976, Feb. 2019, doi: 10.3390/ijms20040976.
- [5] S. K. Sahoo, B. Manoharan, and N. Sivakumar, "Chapter 1 - Introduction: Why Perovskite and Perovskite Solar Cells?," in *Perovskite Photovoltaics*, Elsevier, 2018, pp. 1–24, doi: 10.1016/b978-0-12-812915-9.00001-0.
- [6] W. Chen *et al.*, "Eliminating J-V hysteresis in perovskite solar cells via defect controlling," *Organic Electronics*, vol. 58, pp. 283–289, Jul. 2018, doi: 10.1016/j.orgel.2018.04.017.
- [7] R. Guo *et al.*, "Initial Stages of Photodegradation of MAPbI₃ Perovskite: Accelerated Aging with Concentrated Sunlight," *Solar RRL*, vol. 4, no. 2, Jul. 2019, doi: 10.1002/solr.201900270.
- [8] A. G. Boldyreva *et al.*, "Impact of charge transport layers on the photochemical stability of MAPbI₃ in thin films and perovskite solar cells," *Sustainable Energy & Fuels*, vol. 3, no. 10, pp. 2705–2716, 2019, doi: 10.1039/c9se00493a.
- [9] F. Khorramshahi and A. Takshi, "Ion Migration Magnified Photoresponse in Perovskite Devices," in *2019 IEEE 46th Photovoltaic Specialists Conference (PVSC)*, Jun. 2019, doi: 10.1109/pvsc40753.2019.8980736.
- [10] E.-W. Chang, J.-Y. Huang, and Y.-R. Wu, "Analysis of the hysteresis effect in Perovskite solar cells for the traditional and inverted architectures," in *2020 47th IEEE Photovoltaic Specialists Conference (PVSC)*, Jun. 2020, doi: 10.1109/pvsc45281.2020.9300759.
- [11] N. Lu, J. Wang, D. Geng, L. Li, and M. Liu, "Understanding the transport mechanism of organic-inorganic perovskite solar cells: The effect of exciton or free-charge on diffusion length," *Organic Electronics*, vol. 66, pp. 163–168, Mar. 2019, doi: 10.1016/j.orgel.2018.12.007.
- [12] M. T. Neukom *et al.*, "Consistent Device Simulation Model Describing Perovskite Solar Cells in Steady-State, Transient, and Frequency Domain," *ACS Applied Materials & Interfaces*, vol. 11, no. 26, pp. 23320–23328, Jun. 2019, doi: 10.1021/acsami.9b04991.
- [13] M. T. Khan, M. Salado, A. Almohammadi, S. Kazim, and S. Ahmad, "Elucidating the Impact of Charge Selective Contact in Halide Perovskite through Impedance Spectroscopy," *Advanced Materials Interfaces*, vol. 6, no. 21, Sep. 2019, doi: 10.1002/admi.201901193.
- [14] N. S. Singh, L. Kumar, and V. K. Sharma, "Solving the equivalent circuit of a planar heterojunction perovskite solar cell using Lambert W-function," *Solid State Communications*, vol. 337, p. 114439, Oct. 2021, doi: 10.1016/j.ssc.2021.114439.
- [15] P. Liao, X. Zhao, G. Li, Y. Shen, and M. Wang, "A New Method for Fitting Current–Voltage Curves of Planar Heterojunction Perovskite Solar Cells," *Nano-Micro Letters*, vol. 10, no. 1, Oct. 2017, doi: 10.1007/s40820-017-0159-z.
- [16] N. E. Courtier, G. Richardson, and J. M. Foster, "A fast and robust numerical scheme for solving models of charge carrier transport and ion vacancy motion in perovskite solar cells," *Applied Mathematical Modelling*, vol. 63, pp. 329–348, Nov. 2018, doi: 10.1016/j.apm.2018.06.051.
- [17] N. E. Courtier, J. M. Foster, S. E. J. O’Kane, A. B. Walker, and G. Richardson, "Systematic derivation of a surface polarisation model for planar perovskite solar cells," *European Journal of Applied Mathematics*, vol. 30, no. 3, pp. 427–457, Apr. 2018, doi: 10.1017/s0956792518000207.
- [18] P. Roy, Y. Raoui, and A. Khare, "Design and simulation of efficient tin based perovskite solar cells through optimization of selective layers: Theoretical insights," *Optical Materials*, vol. 125, p. 112057, Mar. 2022, doi: 10.1016/j.optmat.2022.112057.
- [19] T. Bendib, H. Bencherif, M. A. Abdi, F. Meddour, L. Dehimi, and M. Chahdi, "Combined optical-electrical modeling of perovskite solar cell with an optimized design," *Optical Materials*, vol. 109, p. 110259, Nov. 2020, doi: 10.1016/j.optmat.2020.110259.
- [20] J. Gong and S. Krishnan, "Simulation of Inverted Perovskite Solar Cells," in *ASME 2018 12th International Conference on Energy Sustainability*, Jun. 2018, doi: 10.1115/es2018-7227.
- [21] W. Clarke, L. J. Bennett, Y. Grudeva, J. M. Foster, G. Richardson, and N. E. Courtier, "IonMonger 2.0: software for free, fast and versatile simulation of current, voltage and impedance response of planar perovskite solar cells," *Journal of Computational Electronics*, Nov. 2022, doi: 10.1007/s10825-022-01988-5.
- [22] A. C. Nkele, I. S. Ike, S. Ezugwu, M. Maaza, and F. I. Ezema, "An overview of the mathematical modelling of perovskite solar cells towards achieving highly efficient perovskite devices," *International Journal of Energy Research*, vol. 45, no. 2, pp. 1496–1516, Sep. 2020, doi: 10.1002/er.5987.
- [23] L. J. Yao, R. Ranom, K. A. Baharin, and N. M. Sarif, "A Review of Perovskite Solar Cell (PSC): Its Revolution and Mathematical Modelling," *ARPJ Journal of Engineering and Applied Sciences*, vol. 18, no. 13, pp. 1590–1608, Sep. 2023, doi: 10.59018/0723199.
- [24] J. M. Foster, H. J. Snaith, T. Leijtens, and G. Richardson, "A Model for the Operation of Perovskite Based Hybrid Solar Cells: Formulation, Analysis, and Comparison to Experiment," *SIAM Journal on Applied Mathematics*, vol. 74, no. 6, pp. 1935–1966, Jan. 2014, doi: 10.1137/130934258.
- [25] R. Ranom, "Mathematical modeling of lithium-ion battery," Ph.D dissertation, School of Science and Mathematics, University of Southampton, 2014, Available: <http://eprints.soton.ac.uk/id/eprint/375538>.
- [26] S. Soedergren, A. Hagfeldt, J. Olsson, and S.-E. Lindquist, "Theoretical Models for the Action Spectrum and the Current-Voltage Characteristics of Microporous Semiconductor Films in Photoelectrochemical Cells," *The Journal of Physical Chemistry*, vol. 98, no. 21, pp. 5552–5556, May 1994, doi: 10.1021/j100072a023.
- [27] D. K. Maram, H. Abnavi, H. Habibiyan, H. Ghafoorifard, and O. Shekoofa, "TDMA Based Numerical Approach on Modeling of Charge Carrier Transport and Ion Vacancy Motion in Perovskite Solar Cells," in *2020 28th Iranian Conference on Electrical*

Engineering (ICEE), Aug. 2020, doi: 10.1109/icee50131.2020.9260762.




- [28] X. Zhang, J.-X. Shen, W. Wang, and C. G. de Walle, "First-Principles Analysis of Radiative Recombination in Lead-Halide Perovskites," *ACS Energy Letters*, vol. 3, no. 10, pp. 2329–2334, Sep. 2018, doi: 10.1021/acsenenergylett.8b01297.
- [29] J. Gong, "Simulation of steady-state characteristics of heterojunction perovskite solar cells in wxAMPS," *Optik*, vol. 232, p. 166382, Apr. 2021, doi: 10.1016/j.ijleo.2021.166382.
- [30] K. Amri, R. Belghouthi, R. Gharbi, and M. Aillerie, "Effect of defect densities and absorber thickness on carrier collection in Perovskite solar cells," in *2020 7th International Conference on Control, Decision and Information Technologies (CoDIT)*, Jun. 2020, doi: 10.1109/codit49905.2020.9263934.

BIOGRAPHIES OF AUTHORS






Saidatul Nur Aisyah Tun Sakinah    obtained her B.Sc. Mechatronics Engineering in year 2018 from the Faculty of Electrical Engineering, Universiti Teknikal Malaysia Melaka. She passed her final year project title "Kinematics Analysis of Fish Robot Movement". She has 2 years of experience in quality assurance for logistics and assembly production at Allied Precision Technologies. Currently, she is pursuing study in M.Sc. research in Faculty of Electrical Technology and Engineering, Universiti Teknikal Malaysia Melaka. She can be contacted at email: m012020012@student.utem.edu.my.






Rahifa Ranom    obtained her Ph.D. in Applied Mathematics from Southampton University, United Kingdom in 2015. Her Ph.D. research was on the mathematical modeling of Li-ion batteries. She is currently a senior lecturer in the Faculty of Technology and Electrical Engineering, Universiti Teknikal Malaysia Melaka, and a researcher under the Energy and Smart Grid Technology Research Group. She secured a Fundamental Research Grant Scheme for research in Perovskite Solar Cell in November 2020. She can be contacted at email: rahifa@utem.edu.my.



Siti Hajar Basmin    obtained her B.Sc. Electrical Engineering in the year 2022 from the Faculty of Electrical Engineering, Universiti Teknikal Malaysia Melaka. She passed her final year project title "The numerical simulation of 1-D Perovskite Solar Cell in Perovskite Layer". Now, she is Quality Engineer at OSI Optoelectronics Sdn. Bhd, PTD 159386 KM6.5 Jalan Kampung Maju Jaya, Jalan Kempas Lama, 81300 Johor Bahru, Johor. She can be contacted at email: sbasmin@osioptoelectronics.com.



Lee Jin Yao    obtained his B.Sc. Electrical Engineering in the year 2020 from the Faculty of Electrical Engineering, Universiti Teknikal Malaysia Melaka. He has 1 year of experience in overseeing the EPCC installation of the NEM PV system project as well as monitoring the O&M process which was carried out by a contractor at UTeM Holdings Sdn Bhd. Currently, he is pursuing study M.Sc. in Electrical Engineering at the Faculty of Electrical Technology and Engineering, Universiti Teknikal Malaysia Melaka. He can be contacted at email: m012120006@student.utem.edu.my.